PAPER

Check for updates

UiO-66 derived ZrO$_2$@C catalysts for the double-bond isomerization reaction of 2-butene

Xiaoping Chen, [ID] [ab] Xianfei Wang, [b] Wei Liu, [b] Hui Tian, [ID] [b] Yupeng Du, [ID] [b] Haisheng Wei [ID] [b] and Linsheng Tang*[a]

1-Butene, as one of the widely used chemical raw materials, can be produced by the double bond isomerization of 2-butene. However, the current yield of the isomerization reaction is only up to 20% or so. It is therefore an urgent issue to develop novel catalysts with higher performances. In this work, a high-activity ZrO$_2$@C catalyst that is derived from UiO-66(Zr) is fabricated. The catalyst is prepared by calcining the precursor UiO-66(Zr) at high temperature in nitrogen, and characterized by XRD, TG, BET, SEM/TEM, XPS and NH$_3$-TPD. The results demonstrate that the calcination temperature has significant influences on the catalyst structure and performance. Regarding the catalyst ZrO$_2$@C-500, the selectivity and yield of 1-butene are 94.0% and 35.1%, respectively. The high performance is due to multiple aspects, including the inherited octahedral morphology from parent UiO-66(Zr), suitable medium-strong acidic active sites and high surface area. The present work will lead to a better understanding of the ZrO$_2$@C catalyst and guide the rational design of high-activity catalysts for the double bond isomerization of 2-butene to 1-butene.

1 Introduction

1-Butene is one of the key raw materials to produce linear low-density polyethylene (LLDPE), high-density polyethylene (HDPE), polybutylene (PB) resins,[1–3] and other chemicals such as sec-butanol[4] and butadiene.[5] Generally, 1-butene is obtained *via* separation from mixed C4 in a fluid catalytic cracking (FCC) unit or the C4 mixture in a steam cracking (SC) plant.[6] Nevertheless, the content of 1-butene in C4 mixtures is commonly low, namely 15–20%. As a matter of fact, the remaining C4 mixture after the separation of 1-butene is rich in 2-butene, including *cis*-2-butene and *trans*-2-butene, which can be just used as a fuel. However, 2-butene can be utilized together with 1-butene to produce methyl ethyl ketone (MEK) *via* the hydration of 1-butene/2-butene[7] or isobutene *via* the skeletal isomerization of the linear butene[8] or propylene *via* butene cross-metathesis.[9] Recently, the conversion of 2-butene into 1-butene *via* double bond isomerization has also been paid much attention in both academia and industry. Typical processes for converting 2-butene to 1-butene include the French Institute of Petroleum (IFP) process,[10,11] the DOW chemical process,[12] the LUMMUS process,[13] and the Shanghai Petrochemical Research Institute process.[14,15]

As the double bond isomerization of 2-butene to 1-butene is an acid catalyzed reaction, the commonly used catalysts are various acid catalysts, such as molecular sieves catalysts,[16,17] metal oxides catalysts,[18] sulphates/phosphates[19] cation exchange resins,[20,21] metal-based catalysts with ionic polymers or metal oxides as support[22–25] are adopted. However, the reported yield of 1-butene is only 20% or so by using these catalysts. And the further separation process for the products and reactants is often by precision distillation or extractive distillation,[26,27] or by absorption with zeolite[28] or MOFs,[29] with a complex process and high energy consumption. Therefore, higher yield of 1-butene can decrease the corresponding energy consumption and economic cost.

Metal organic frameworks (MOFs), as a porous material composed of metal nodes and organically linked ligands, can be utilized as acid catalysts by pre-/post-treatments.[30–33] The unique multidimensional regular pore structure of MOFs makes them a proper choice for catalyst carriers. However, the microporous structure of MOFs limits the physical diffusion of reactants and products, which gives rise to significantly insufficient contact of reactants with the catalytic active site.[34–36] Therefore, increasing the pore diameter, reducing the influence of diffusion on the reaction, and improving the catalytic activity have become hot topics in developing MOF-derived catalysts.[37,38]

The addition of a third substance[39] or the elevated temperature during the synthesis of MOFs[40–43] can disrupt parts of the regular and ordered structures, exposing more active centers and increasing the pore diameter. For instance, Z. Hasan *et al.*[40]

[a]College of Chemical Engineering, Qingdao University of Science and Technology, Qingdao 266042, China. E-mail: linshengt62@163.com

[b]College of Chemistry and Chemical Engineering, Yantai University, Yantai 264005, China

prepared Zirconia–carbon (ZC) *via* calcination of UiO-66 and amino-functionalized UiO-66 under N_2 atmosphere. Li *et al.*[41] prepared a CaO/ZrO_2 catalyst which was derived from the UiO-66 supported calcium acetate. Torad *et al.*[42] obtained Co-based carbon materials by pyrolytic carbonization of ZIF-67 at 800 °C under nitrogen atmosphere. Zhang *et al.*[43] used MIL-125-(Ti) as a precursor and furfuryl alcohol was added in preparation of nano-TiO_2@C composite catalysts under argon atmosphere.

Since UiO-66 is a MOF with good hydrothermal stability and chemical stability,[44–48] and it shows quite high selectivity to 1-butene (97–99%).[49] However, the yield of 1-butene is still low (*i.e.*, 10%) because of the saturated coordination Zr cites. Moreover, as for the acid-treated UiO-66, the Lewis acidity of the catalyst is still weak.[50,51]

The aim of this paper is to develop a high-activity and high-selectivity catalyst through calcination of UiO-66(Zr) at various temperatures. In Section 2, the preparation, characterization, and evaluation of the UiO-66(Zr) derived ZrO_2@C catalysts are presented. In Section 3, the effects of the carbonization temperature on the performances of the catalysts are discussed. In Section 4, conclusions on the ZrO_2@C catalyst are drawn.

2 Experimental

2.1 Raw materials

Zirconium tetrachloride and terephthalic acid are analytically pure, purchased from Shanghai Aladdin Biochemical Technology Co., Ltd. *N,N*-dimethylformamide, hydrochloric acid and acetic acid are analytically pure, purchased from Sinopharm Group Chemical Reagents Co., Ltd 2-Butene is purchased from Dalian Special Gases Co., Ltd The mass percentage of 2-butene is: *cis*-2-butene 97.28%, *trans*-2-butene 2.48%, 1-butene 0.06%, isobutene 0.18%.

2.2 Catalyst preparation

2.2.1 Preparation of UiO-66. The UiO-66 catalyst is further optimized based on the synthesis methods reported by Katz[52] and Destefano[53] *et al.* The preparation process is as follows: 0.932 g (4 mmol) zirconium tetrachloride ($ZrCl_4$) is dissolved in 24 ml *N,N*-dimethylformamide (DMF), and 0.997 g (6 mmol) terephthalic acid (H_2BDC) is added after 30 min of ultrasound until dissolved. The ultrasound is continued until completely dissolved and 0.66 ml hydrochloric acid and 21.6 ml acetic acid are added. The mixture solution is transferred to a 100 ml polytetra-fluoroethylene reactor, and the reactor is placed in a microwave hydrothermal parallel synthesizer. The temperature is programmed to 150 °C at the rate of 10 °C min^{-1} for 2 h. After the material is cooled to room temperature, it is centrifuged. The solid is washed three times with DMF and methanol respectively, and then dried in a vacuum drying oven at 150 °C for 24 h. The white powder is UiO-66.

2.2.2 Preparation of ZrO2@C. Under the condition of continuous nitrogen injection (nitrogen flow rate is 200 ml min^{-1}) and Muffle furnace heating rate is 10 °C min^{-1}, the UiO-66 sample in crucible is roasted at a certain temperature for
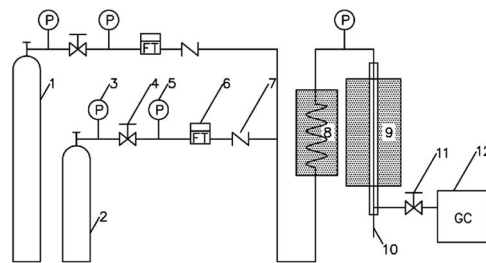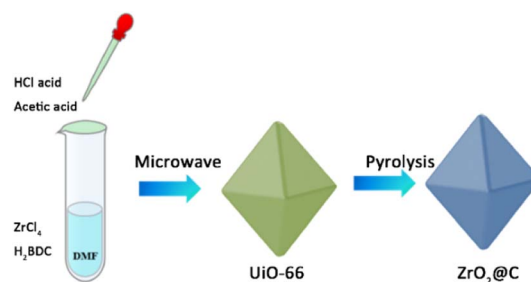

Fig. 1 A setup for catalyst evaluation. (1) Nitrogen cylinder; (2) raw material cylinder; (3) primary pressure gauge; (4) pressure regulating valve; (5) two-stage pressure gauge; (6) mass flowmeter; (7) check valve; (8) feed preheater; (9) reactor; (10) thermometer; (11) back pressure valve; (12) on-line gas chromatograph.

Scheme 1 Illustration of the synthesized process of ZrO_2@C catalyst.

2 h. Samples roasted at 400, 500, 600 and 700 °C are labelled as ZrO_2@C-400, ZrO_2@C-500, ZrO_2@C-600 and ZrO_2@C-700, respectively. These catalysts are called as ZrO_2@C-*X* catalysts, where the *X* refers to the specific calcination temperature.

2.3 Catalyst characterization and evaluation

X-ray diffraction measurements (XRD) of solid samples are carried out on a SmartLab 6000 X-ray diffractometer by using Cu Kα radiation (α = 0.15418 nm) from 10.0° to 80.0°.

JSM-7900F field emission – scanning electron microscopy (FE-SEM) and FEI Joel F200 transmission election microscopy (TEM) are employed to observe the micro morphology of catalyst samples.
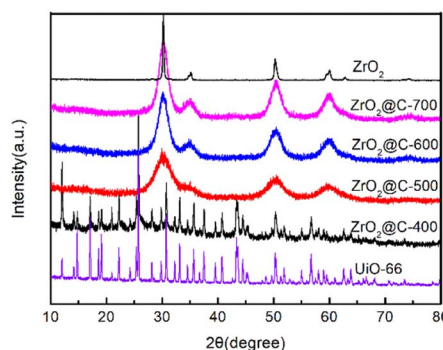

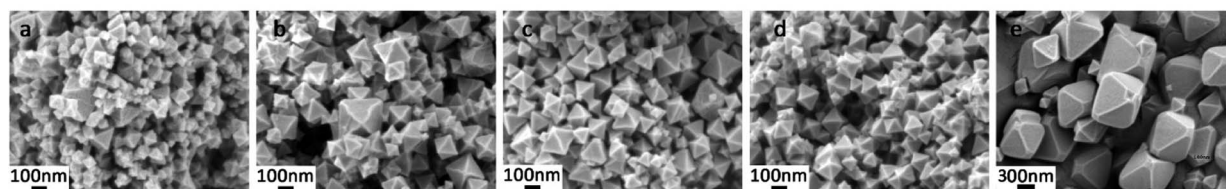
Fig. 2 XRD spectra of UiO-66, ZrO_2 and ZrO_2@C-*X* catalysts.

Fig. 3 SEM images of ZrO$_2$@C-X catalysts: (a). ZrO$_2$@C-400, (b). ZrO$_2$@C-500, (c). ZrO$_2$@C-600, (d). ZrO$_2$@C-700, (e). UiO-66.

N$_2$ adsorption–desorption isotherms are tested on a Micromeritics ASAP 2020 gas-sorption apparatus at −196 °C. The specific surface area is determined with the BET model.

X-ray photoelectron spectroscopy (XPS) of the samples is carried out on a Thermo Fisher ESCALAB Xi+ apparatus.

NH$_3$-TPD adsorption/desorption investigations are carried out by AutoChem II 2920 adsorption instrument equipped with a thermal conductivity detector (TCD). The strength of acid sites is analyzed from the position temperature of TPD signals.

Thermal gravimetric (TG) analysis in air is performed by using NETZSCH STA 449 F5 to determine the amount of carbon in the prepared catalysts. The air flowrate is 50 ml min^{-1}. The heating rate is 10 °C min^{-1}.

Elements analyse is performed by using an Agilent 5100 ICP spectrometer. The RF Power is 1150, plasma flow is 12 L min^{-1}, sample uptake delay time is 12 s.

Pyridine IR (Py-IR) is carried out by Thermo Fisher Nicolet iS50. The heating rate is 10 °C min^{-1} up to the measured temperature (fixed point temperature of 250 °C and 350 °C respectively) for vacuum desorption for 0.5 h.

The performance of catalytic double bond isomerization of butene is evaluated in a fixed-bed setup as shown in Fig. 1.

The catalyst particle size is 40–60 mesh, the catalyst filling volume is 6 ml, and both ends of the reaction tube are filled with quartz sand. The feedstock feed flow rate is controlled by a mass flowmeter. The reaction pressure is normal pressure. The outlet of the reactor is filtered into the on-line Agilent GC8890 gas chromatography for real-time analysis. The detection conditions are as follows: six-way valve automatic injection, hydrogen flame detector (FID), HP PLOT/Al$_2$O$_3$ column (50 m × 0.53 mm × 15 μm), carrier gas N$_2$, column oven temperature 100 °C, quantification by area normalization method.

3 Results and discussion

As shown in Scheme 1, the UiO-66 precursor is prepared by a modified microwave method, in which the acetic acid is added to adjust the structure. The obtained UiO-66 is further calcined at various temperature under N$_2$ atmosphere and the corresponding product is denoted as ZrO$_2$@C-X. The calcination temperature of ZrO$_2$@C-X catalyst is investigated in detail. The results in Fig. 2 show that the sample calcined at 400 °C keeps the same diffraction peaks with UiO-66 precursor, indicating that the structure of UiO-66 is not decomposed, which happens at the temperature higher than 400 °C, such as 500, 600, 700 °C. It is observed that the ZrO$_2$@C-500, ZrO$_2$@C-600 and ZrO$_2$@C-700 samples present the diffraction peaks of ZrO$_2$(PDF#88-

1007), in which 30.3°, 35.2°, 50.3°, 60.2° and 62.9° belong to the (101), (110), (112), (211) and (202) crystal face, respectively. Moreover, it is found that higher calcination temperature results in more acute diffraction peak, suggesting the formation of larger particles, which are confirmed by SEM characterization. As shown in Fig. 3, the samples calcined at various temperature exhibit the same structure of UiO-66, and the size of ZrO$_2$@C-X crystal is 100–200 nm (Fig. 3a–d) while UiO-66 is about 500 nm (Fig. 3e), consistent with XRD results. In Z. Hasan's work,[40] the optimal calcination temperature is 900 °C at which will cause the structure of UiO-66 decomposed. In this work, the highest calcination temperature is 700 °C.

The pore structures of various ZrO$_2$@C-X catalysts are analyzed by N$_2$ adsorption–desorption experiments. The results in Fig. 4a display that ZrO$_2$@C-400 catalyst mainly possesses the microporous structure as that in UiO-66 precursor and high surface area of 809.0 m^2 g^{-1}, agreement with XRD results. When the samples are calcined at higher temperature (*i.e.*, 500, 600, 700 °C), the adsorption–desorption isotherms curves belong to type IV, with obvious H3 hysteresis loop and no obvious saturated adsorption capacity, indicating that the material has
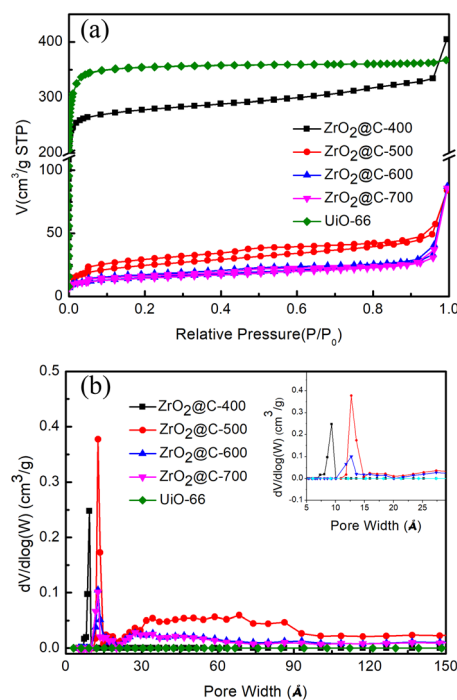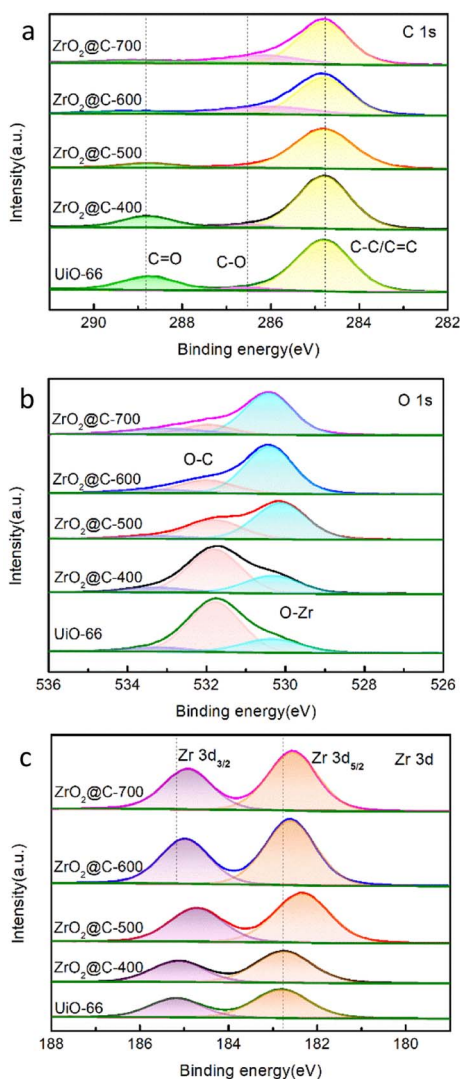

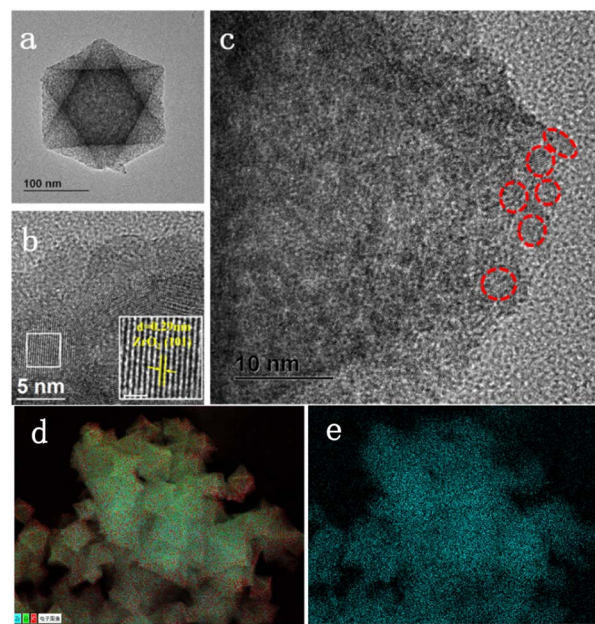**Fig. 4** (a) N$_2$ adsorption–desorption curves. (b) pore distribution of ZrO$_2$@C-X catalysts.

Table 1 Specific surface area and pore volume of ZrO_2@C-X catalysts

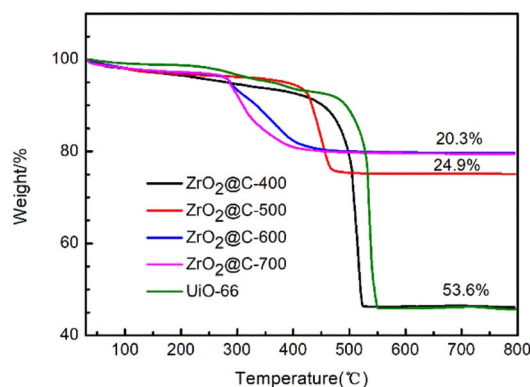| Catalyst	S_{BET} (m^2 g^{-1})	V_{micro} (cm^3 g^{-1})	V_{total} (cm^3 g^{-1})
ZrO_2@C-400	809.0	0.356	0.493
ZrO_2@C-500	84.3	0.009	0.074
ZrO_2@C-600	50.6	0.007	0.044
ZrO_2@C-700	48.9	0.006	0.041
UiO-66	1070.4	0.512	0.559

Fig. 6 HRTEM images of ZrO_2@C-500 catalyst at different scale bar ((a)100 nm; (b) 5 nm; (c) 10 nm; (d and e) total element distribution; (f) Zr distribution).

Fig. 5 XPS analysis of the ZrO_2@C-X catalysts. (a). C 1s, (b). O 1s, (c). Zr 3d.

mesoporous structure.[54,55] As the calcination temperature increases, the microporous structure decreases and the mesoporous structure emerges, which is due to the decomposition of more organic ligands. Meanwhile, the surface area sharply decreases under 100 m^2 g^{-1}, which is 84.3, 50.6, 48.9 m^2 g^{-1} for ZrO_2@C-500, ZrO_2@C-600 and ZrO_2@C-700 (Table 1), respectively. Among above catalysts, ZrO_2@C-500 sample owns the highest surface area and broader pore size distribution (Fig. 4b), which favours the improvement of catalytic performance.

ZrO_2@C-500 is further studied by X-ray photoelectron spectroscopy (XPS) analysis. As shown in Fig. 5, the XPS results exhibit the peaks corresponding to C 1s, O 1s and Zr 3d. C 1s peak fitting results show three peaks at 288.8, 286.7 and 284.8 eV corresponding to C=O, C–O and C–C/C=C, respectively. O 1s peaks also display three bands at 533.3, 531.8 and 530.1 eV for oxygen of O=C, O–C and O–Zr, respectively. The Zr 3d peaks show two peaks at 182.4 eV (Zr–O) and 184.7 eV referring to Zr 3d$_{3/2}$.[56] XPS analysis verifies the element component of ZrO_2@C catalyst. With the increase of calcination temperature, the content of C–C/C=C and C=O, especially the content of C=O bond decreases as shown in the C 1s spectrum (Fig. 5a)., the content of C–O bond decreases while the content of O–Zr bond increases significantly shown in the O 1s spectrum (Fig. 5b), Zr 3d$_{3/2}$ and Zr 3d$_{5/2}$ has the same increasable tendency shown in the Zr 3d spectrum (Fig. 5c). These appearances are attributed to the pyrolysis and carbonization of organic ligands in UiO-66 at the specified calcination temperature.

The morphology of ZrO_2@C-500 catalyst is further analyzed by HRTEM characterization. As shown in Fig. 6, the sample still contains the octahedral structure and presents abundant white spots, which is attributed to the porous structure. In addition, the crystal lattice of 0.29 nm is clearly observed in the catalyst, which is corresponding to the (101) face in ZrO_2, consistent with XRD results. Moreover, the images show that ZrO_2 nanoparticles are embedded in the carbon support. Uniform distribution of element Zr over C can be observed in Fig. 6d and e. Therefore, combining with XPS results, the obtained materials can be denoted as ZrO_2@C structure.[57]
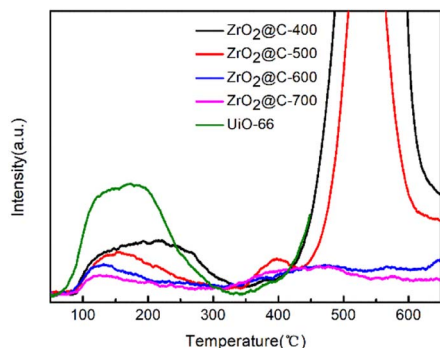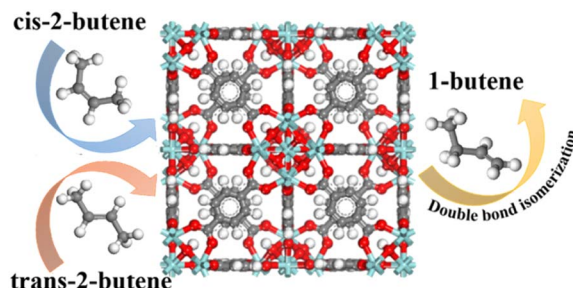
Fig. 7 NH$_3$-TPD spectra of ZrO$_2$@C-X catalysts.
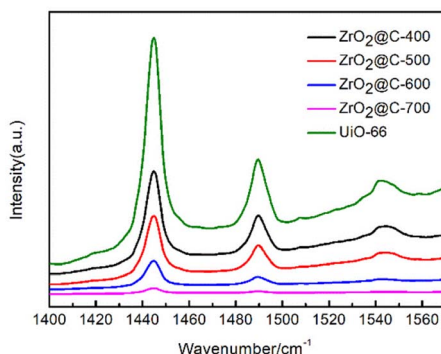
Fig. 8 Pyridine infrared of ZrO$_2$@C-X catalysts.

Fig. 9 TG analyses of ZrO$_2$@C-X catalysts.

Table 2 The contents of Zr in ZrO$_2$@C-catalysts

Catalyst	Content of Zr in catalyst, wt%
ZrO$_2$@C-400	18.01
ZrO$_2$@C-500	20.67
ZrO$_2$@C-600	27.65
ZrO$_2$@C-700	34.70
UiO-66	37.52

Scheme 2 The double bond isomerization of 2-butene to 1-butene.

Fig. 10 (a) Catalytic performance of ZrO$_2$@C-X catalysts for the isomerization of 2-butene, (b) stability test result of ZrO$_2$@C-500.
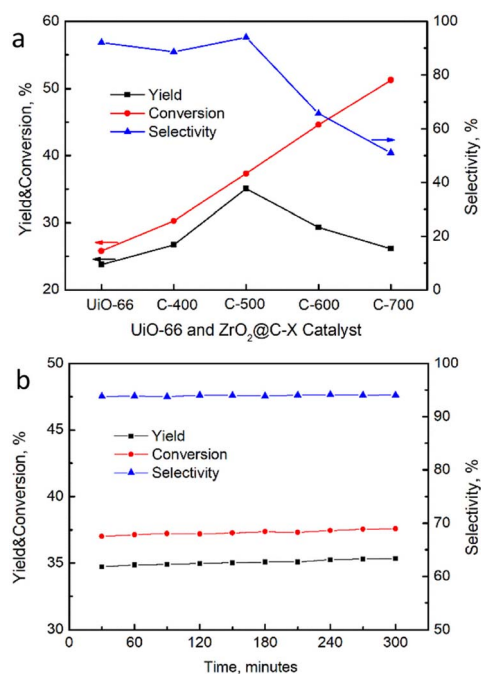
As for the isomerization reaction, the acid sites play an important role in the catalytic performance. So, the acidic property of ZrO$_2$@C-X catalysts are studied by NH$_3$-TPD experiments. The results in Fig. 7 show that the catalysts calcined at different temperature have diverse acidic sites. In general, the acidic sites are divided into weak, medium and strong acidic sites corresponding to the NH$_3$ desorption temperature at the range of $\leq$200 °C, 200–350 °C, $\geq$350 °C, respectively. The ZrO$_2$@C-400 catalyst exhibiting different NH$_3$ desorption profiles results from the decomposition of organic ligand. For other calcined catalysts, the higher calcined temperature

decreases the content of weak acid species, where ZrO$_2$@C-500 catalyst owns the highest amount of weak acid sites. Meanwhile, ZrO$_2$@C-500 catalyst exists obvious medium strong acidic species at around 400 °C. And the NH$_3$ desorption curve at higher than 450 °C is due to the pyrolyzation of residual organic ligand. For ZrO$_2$@C-600 and ZrO$_2$@C-700 catalysts, they present more strong acidic species at temperature higher than

Table 3 Products distribution of the isomerization of 2-butene on ZrO_2@C-X catalysts (under the reaction conditions of 390 °C and 48 h^{-1})

Product	ZrO_2@C-400	ZrO_2@C-500	ZrO_2@C-600	ZrO_2@C-700	UiO-66
<C3	3.55	2.10	32.46	47.63	2.23
Isobutene	0.76	0.11	0.35	0.38	0.12
>C5	7.12	3.76	1.48	0.96	5.53
1-Butene	88.57	94.03	65.71	51.03	92.12

450 °C, which is attributed to the decrease content of encapsulated carbon.

According to the results of pyridine infrared (Fig. 8), the prepared ZrO_2@C catalysts retain a large number of UiO-66 organic ligands (terephthalic acid) when the calcination temperature is below 400 °C, resulting in a total acid content higher than that of the catalyst calcined at 500 °C or above. For the Zr@C-500, Zr@C-600 and Zr@C-700 catalysts, it is inferred that the B acid plays a major role in the reaction due to its high total acid content and high B/L in Zr@C-500. Both organic (such as C–O or C–C, *etc.*) and inorganic (such as Pd or Zr, *etc.*) sites can be the activity sites,[22–25] just as the ZrO_2@C catalysts in this work.

This phenomenon is further confirmed by TG analysis in Fig. 9. The ZrO_2@C-400 catalyst exhibits 53.6% weight loss due to the decomposition of unpyrolyzed ligand. The weight loss remarkably descends to 24.9% and 20.3% for ZrO_2@C-500 and ZrO_2@C-600 catalysts. Therefore, ZrO_2@C-500 catalyst possesses more carbon content than that in ZrO_2@C-600 and ZrO_2@C-700 samples, which cover more strong acidic species by the encapsulated structure.

The contents of element Zr in ZrO_2@C-catalysts are determined by ICP as shown in Table 2. The contents of zirconium element increase with the increase of calcination temperature, indicating that more organic ligands are burned off as the calcination temperature increases.

The catalytic performance of resultant catalysts was performed in the isomerization of 2-butene to 1-butene under the reaction conditions of 390 °C and 48 h^{-1}, which was optimized in our previous work with a similar MOF-derived catalyst.[49] Both *cis*-2-butene and *trans*-2-butene might be converted to 1-butene as shown in Scheme 2. The yield of reference catalyst UiO-66 was declined 2% in 300 minutes, while conversion and selectivity on the ZrO_2@C catalysts had no obvious change in the equally reaction time. All the catalysts performance reaction time were 300 minutes referenced to UiO-66. As shown in Fig. 10a, the conversion of 2-butene increases along with the calcination temperature, which might be due to the exposure of more strong acidic sites on the catalysts, as verified by the NH$_3$-TPD results. However, the selectivity of 1-butene appears volcanic shape, in which ZrO_2@C-500 catalyst shows the best selectivity, achieving 94.0% conversion and 35.1% yield of 1-butene, better than the yield of 18–20% in the reported literature [8–14], which is ascribed to the exposure of suitable acidic species by encapsulated carbon and relatively high surface area. Moreover, the product distribution demonstrates that the stronger acidic sites in ZrO_2@C-600 and ZrO_2@C-700 catalysts lead to the cracking of 2-butene to the by-product of C3

component (Table 3), which further explains the high selectivity of ZrO_2@C-500 catalyst. In addition, ZrO_2@C-500 catalyst also displays good stability in the 300 min test (Fig. 10b), coming from the unique structure of ZrO_2@C.

4 Conclusions

The ZrO_2@C-X catalysts are fabricated from the UiO-66(Zr) precursor which are calcinated at various temperature under N$_2$ atmosphere. The catalysts with carbon encapsulated ZrO_2 particles are characterized or evaluated using combined techniques, including XRD, SEM, TEM, XPS, FT-IR, TG, ICP, Py-IR and a fixed-bed reactor. Experimental findings indicate that the ZrO_2@C-X catalysts exhibit different catalytic performance while it is calcined at various temperatures. The catalyst ZrO_2@C-500 shows the best catalytic performance for the isomerization of 2-butene to 1-butene, namely, 94.0% conversion of 2-butene and 35.1% yield of 1-butene. The reason can be ascribed to the suitable acidic sites and high surface area in ZrO_2@C-500 which are beneficial for the isomerization reaction. In sum, this work provides a novel strategy to design high-activity acidic catalyst for the isomerization of 2-butene to 1-butene. The approach is expected to be applied to the synthesis of other acid catalysts.

Conflicts of interest

There are no conflicts to declare.

Acknowledgements

Notes and references

1 N. Sood, M. K. Jha and S. Bajpai, *SPE Polym.*, 2021, **2**, 325–335.
2 B. R. Barnett, S. T. Parker, M. V. Paley, M. I. Gonzalez, N. Biggins, J. Oktawiec and J. R. Long, *J. Am. Chem. Soc.*, 2019, **141**, 18325–18333.
3 X. Qiu, C. Hu, J. Li, D. Huang and S. Jiang, *CrystEngComm*, 2019, **21**, 4243–4249.
4 J. G. Cai, *Sci. Discovery*, 2016, **4**, 137–141.
5 W. C. White, *Chem.-Biol. Interact.*, 2007, **166**, 10–14.
6 D. Z. Gao, Y. Hu, D. L. Kong and J. S. Jin, *Contemp. Chem. Ind.*, 2004, **33**, 129–133.

7   E. Sánchez-Ramírez, H. Alcocer-García, A. G. Romero-García, G. Contreras-Zarazua and J. G. Segovia-Hernandez, in *31st European Symposium on Computer Aided Process Engineering*, 2021, pp. 399–405, DOI: 10.1016/b978-0-323-88506-5.50063-2.

8   Y. Hu, C. Xu, H. Zhang, Y. Wang, J. Deng and H. Zhang, *ChemistrySelect*, 2017, **2**, 3408–3413.

9   E. Mazoyer, K. C. Szeto, J. M. Basset, C. P. Nicholas and M. Taoufik, *Chem. Commun.*, 2012, **48**, 3611–3613.

10 M. D. Commereuc, F. B. Didillon, R. H. Olivier-Bourbigou and L. S. C. s. Seine, Production of High Purity Isobutene and Propylene from Hydrocarbon Fractions with Four Carbon Atoms, *US Pat.*, Institut Francais du Petrole, Rueil-Malmaison (FR), 6686510B2, 2004.

11 P. M. Dorbon, V. F. Hugues, V. J.-C. Viltard, R. B. Didillon, A. F. Vernaison, Process for Obtaining Butene-1, *US Pat.*, Institut Francais du Petrole, Rueil-Malmaison (FR), 6242662, 2001.

12 O. Forlani, F. Ancilltti, B. Jover, G. Resofszki and G. Gati, *Appl. Catal.*, 1991, **67**, 237–247.

13 R. J. Gartside, M. I. Greene and H. Kaleem, *Hydrocarbon Process.*, 2006, **85**, 57–61.

14 C. L. Wu, *Coal Chem. Ind.*, 2021, **44**, 129–131.

15 L. Li, Z. Y. Zhu and J. T. Liu, *Chem. React. Eng. Technol.*, 2014, **30**, 342–346.

16 J.-K. Jeon, H. Lee, J.-H. Yim, Y. S. Kim, S. J. Lee, Y.-K. Park, J. K. Shon and J. M. Kim, *Catal. Lett.*, 2007, **119**, 179–184.

17 N. You, J. H. Yim, S. J. Lee, J. H. Lee, Y. K. Park and J. K. Jeon, *J. Nanosci. Nanotechnol.*, 2007, **7**, 3800–3804.

18 Y.-K. Park, S. J. Kim, N. You, J. Cho, S. J. Lee, J. H. Lee and J.-K. Jeon, *J. Ind. Eng. Chem.*, 2011, **17**, 186–190.

19 P. M. Słomkiewicz, *Appl. Catal., A*, 2006, **301**, 232–240.

20 A. Moronta, J. Luengo, Y. Ramírez, J. Quiñónez, E. González and J. Sánchez, *Appl. Clay Sci.*, 2005, **29**, 117–123.

21 P. M. Slomkiewicz, *React. Funct. Polym.*, 1997, **33**, 299–304.

22 Y. Jing, Y. Wang, S. Furukawa, J. Xia, C. Sun, M. J. Hulsey, H. Wang, Y. Guo, X. Liu and N. Yan, *Angew. Chem., Int. Ed. Engl.*, 2021, **60**, 5527–5535.

23 S. Ding, Y. Guo, M. J. Hülsey, B. Zhang, H. Asakura, L. Liu, Y. Han, M. Gao, J.-y. Hasegawa, B. Qiao, T. Zhang and N. Yan, *Chem*, 2019, **5**, 3207–3219.

24 K. Wang, W. Cui, Z. Bian, Y. Liu, S. Jiang, Y. Zhou and J. Wang, *Appl. Catal., B*, 2021, **281**.

25 Q. Wang, X. Ling, T. Ye, Y. Zhou and J. Wang, *J. Mater. Chem. A*, 2019, **7**, 19140–19151.

26 B. Kolbe and S. Wenzel, *Chem. Eng. Process.*, 2004, **43**, 339–346.

27 R. M. Aldossary, R. M. N. Shaik, R. K. A. Al-Majnouni, R. A. Alzenaidi, D. F. Rahman, D. A. Palani, Y. S. Asaoka, D. M. A. Al Yami, D. U. Baduruthamal, Separation of Olefin Components from a Mixture of Butanes and Butenes Using Distillation and Adsorbents, *US Pat.*, Sabic Global Technologies B.V, Bergen op Zoom (NL), 2022.

28 B. Tijsebaert, C. Varszegi, H. Gies, F. S. Xiao, X. Bao, T. Tatsumi, U. Muller and D. De Vos, *Chem. Commun.*, 2008, 2480–2482.

29 Y. He, W. Zhou, R. Krishna and B. Chen, *Chem. Commun.*, 2012, **48**, 11813–11831.

30 S. A. Ivko, T. Bailey, L. Brammer and A. Haynes, *Chem. Commun.*, 2022, **58**, 11252–11255.

31 M. D. Satoshi Horike, K. Tamaki and J. R. Long, *J. Am. Chem. Soc.*, 2008, **130**, 5854–5855.

32 Z. U. Zango, N. S. Sambudi, K. Jumbri, N. H. H. Abu Bakar, N. A. F. Abdullah, E.-S. M. Negim and B. Saad, *Chem. Eng. Sci.*, 2020, 220.

33 M. Mukoyoshi and H. Kitagawa, *Chem. Commun.*, 2022, **58**, 10757–10767.

34 B. Li, K. Leng, Y. Zhang, J. J. Dynes, J. Wang, Y. Hu, D. Ma, Z. Shi, L. Zhu, D. Zhang, Y. Sun, M. Chrzanowski and S. Ma, *J. Am. Chem. Soc.*, 2015, **137**, 4243–4248.

35 J. Chen, R. Liu, Y. Guo, L. Chen and H. Gao, *ACS Catal.*, 2014, **5**, 722–733.

36 R. A. Perlata, M. T. Huxley, Z. Shi, Y.-B. Zhang, C. J. Sumby and C. J. Doonan, *Chem. Commun.*, 2020, **56**, 15313–15316.

37 N. F. H. Nik Zaiman, N. Shaari and N. A. M. Harun, *Int. J. Energy Res.*, 2021, **46**, 471–504.

38 R. R. Salunkhe, Y. V. Kaneti, J. Kim, J. H. Kim and Y. Yamauchi, *Acc. Chem. Res.*, 2016, **49**, 2796–2806.

39 M. K. Alavijeh and M. M. Amini, *Polyhedron*, 2019, 173.

40 Z. Hasan, D. W. Cho, I. H. Nam, C. M. Chon and H. Song, *Materials*, 2016, **9**, 1–14.

41 H. Li, Y. Wang, X. Ma, M. Guo, Y. Li, G. Li, P. Cui, S. Zhou and M. Yu, *Renewable Energy*, 2022, **185**, 970–977.

42 N. L. Torad, M. Hu, S. Ishihara, H. Sukegawa, A. A. Belik, M. Imura, K. Ariga, Y. Sakka and Y. Yamauchi, *Small*, 2014, **10**, 2096–2107.

43 X. Zhang, Y. Liu, Y. Pang, M. Gao and H. Pan, *J. Mater. Chem. A*, 2014, **2**, 1847–1854.

44 P. Ponchai, K. Adpakpang, S. Thongratkaew, K. Chaipojjana, S. Wannapaiboon, S. Siwaipram, K. Faungnawakij and S. Bureekaew, *Chem. Commun.*, 2020, **56**, 8019–8022.

45 A. A. Mohammadi, A. Alinejad, B. Kamarehie, S. Javan, A. Ghaderpoury, M. Ahmadpour and M. Ghaderpoori, *Int. J. Environ. Sci. Technol.*, 2017, **14**, 1959–1968.

46 Y. Wang, N. Zhang, D. Chen, D. Ma, G. Liu, X. Zou, Y. Chen, R. Shu, Q. Song and W. Lv, *Sci. Total Environ.*, 2019, **682**, 118–127.

47 G. C. Shearer, S. Chavan, S. Bordiga, S. Svelle, U. Olsbye and K. P. Lillerud, *Chem. Mater.*, 2016, **28**, 3749–3761.

48 J. Winarta, B. Shan, S. M. McIntyre, L. Ye, C. Wang, J. Liu and B. Mu, *Cryst. Growth Des.*, 2019, **20**, 1347–1362.

49 X. Wang, W. Liu, L. Tian, P. Li, X. Chen and W. Ren, *Pet. Process. Petrochem.*, 2022, **53**, 21–27.

50 M. Kandiah, M. H. Nilsen, S. Usseglio, S. Jakobsen, U. Olsbye, M. Tilset, C. Larabi, E. A. Quadrelli, F. Bonino and K. P. Lillerud, *Chem. Mater.*, 2010, **22**, 6632–6640.

51 M. Stojković and I. A. Pašti, *Catalysts*, 2021, **11**, 264.

52 M. J. Katz, Z. J. Brown, Y. J. Colon, P. W. Siu, K. A. Scheidt, R. Q. Snurr, J. T. Hupp and O. K. Farha, *Chem. Commun.*, 2013, **49**, 9449–9451.

53 M. R. Destefano, T. Islamoglu, S. J. Garibay, J. T. Hupp and O. K. Farha, *Chem. Mater.*, 2017, **29**, 1357–1361.

54 Y. Tao, H. Kanoh., A. Lloyd and K. Kaneko, *Chem. Rev.*, 2006, 896–910.

55 M. Athar, P. Rzepka, D. Thoeny, M. Ranocchiari and J. Anton van Bokhoven, *RSC Adv.*, 2021, **11**, 38849–38855.

56 M. N. Goda, H. N. Abdelhamid and A. E. A. Said, *ACS Appl. Mater. Interfaces*, 2020, **12**, 646–653.

57 J. Joo, T. Yu, Y. W. Kim, H. M. Park, F. Wu, J. Z. Zhang and T. Hyeon, *J. Am. Chem. Soc.*, 2003, **125**, 6553–6557.